ACS APPLIED MATERIALS & INTERFACES

Research Article

www.acsami.org

Functionalized Multiwalled Carbon Nanotubes as Carriers of Ruthenium Complexes to Antagonize Cancer Multidrug Resistance and Radioresistance

Ni Wang,† Yanxian Feng,† Lilan Zeng, Zhennan Zhao, and Tianfeng Chen*

Department of Chemistry, Jinan University, Guangzhou 510632, China

Supporting Information

ABSTRACT: Multidrug resistance and radioresistance are major obstacles for successful cancer therapy. Due to the unique characteristics of high surface area, improved cellular uptake, and the possibility to be easily bound with therapeutics, carbon nanotubes (CNTs) have attracted increasing attention as potential nanodrug delivery systems. In this study, a CNT-based radiosensitive nanodrug delivery system was rationally designed to antagonize the multidrug resistance in hepatocellular carcinoma. The nanosystem was loaded with a potent anticancer ruthenium polypyridyl complex (RuPOP) via $\pi-\pi$ interaction and formation of a hydrogen bond. The functionalized nanosystem (RuPOP@MWCNTs) enhanced the cellular uptake of RuPOP in liver cancer cells, especially drug-resistant R-HepG2 cells, through endocytosis. Consistently, the selective cellular uptake endowed the nanosystem amplified anticancer efficacy against R-HepG2 cells but not in normal cells. Interestingly, RuPOP@MWCNTs significantly enhanced the anticancer efficacy of clinically used X-ray against R-HepG2 cells through induction of apoptosis and G0/G1 cell cycle arrest, with the involvement of ROS overproduction, which activated several downstream signaling pathways, including DNA damage-mediated p53 phosphorylation, activation of p38, and inactivation of AKT and ERK. Moreover, the nanosystem also effectively reduces the toxic side effects of loaded drugs and prolongs the blood circulation *in vivo*. Taken together, the results demonstrate the rational design of functionalized carbon nanotubes and their application as effective nanomedicine to overcome cancer multidrug resistance.

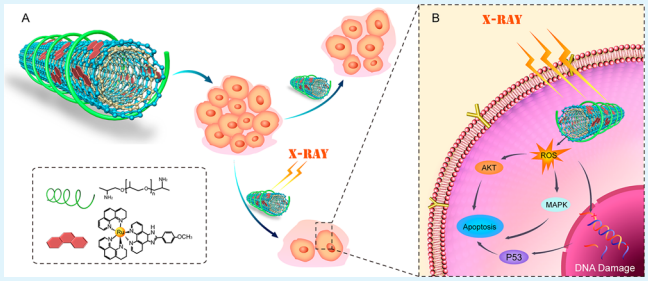

KEYWORDS: *carbon nanotube, drug delivery system, anticancer, drug resistance, radioresistance*

INTRODUCTION

There have been tremendous efforts to conquer cancer with current chemotherapy. However, previous treatment has induced severe side effects in patients, such as diarrhea, sickness, hair loss, myelosuppression, and cardio toxicity.[1,2] Studies have showed that inhibition of the multidrug resistance (MDR) ability of resistant cancer cells would be a good way to achieve successful cancer therapy and to decrease the dose of anticancer drugs.[3,4] In order to reduce the clinically used drug dosage and side effects, drug-delivery systems (DDS) have been developed to overcome this problem because they offered excellent efficient drug transportation. Nanotechnology-based drug delivery systems (NDDS), such as polymer nanoparticles, gold nanoparticles, mesoporous silica nanoparticles, liposomal, and titanium nanostructures, have been considered to decrease efflux from different cancer cells.[5−12] Due to the enhanced permeability and retention (EPR) effect or active targeting delivery, nanocarriers loaded with therapeutics can accumulate at the parts of tumors, which could increase the effects of chemotherapeutics and decrease the toxic side effects. NDDS are becoming more and more applied in cancer therapy and diagnosis.[13,14]

Over the years, a large number of various nanocarriers have been constructed and synthesized, such as gold nanoparticles, mesoporous silica nanoparticles, graphene, polymer nanoparticles, and carbon nanotubes.[8,9,15−18] Among these nanosystems, carbon nanotubes (CNTs) consisting of allotropes of carbon with cylindrical nanostructure have recently gained tremendous attention in biomedical applications.[19] CNTs are well-ordered, with an excellent aspect ratio, surface area, mechanical strength, ultralight weight, and admirable thermal and chemical stability.[20] On the basis of these behaviors, CNTs turn into potential nanomaterial for biomedical applications. It has been generally accepted that drugs with aromatic groups could be adsorbed to CNTs easily in a noncovalent mode through $\pi-\pi$ stacking.[21] Studies have found that doxorubicin (DOX) is commonly used as an anticancer drug, which could be loaded onto the single-walled carbon nanotubes (SWCNTs) via $\pi-\pi$ stacking interaction.[22] The CNT-based drug delivery system passed through the cell membrane, and then DOX

Received: April 29, 2015
Accepted: June 24, 2015
Published: June 24, 2015

DOI: 10.1021/acsami.5b03739
ACS Appl. Mater. Interfaces 2015, 7, 14933−14945

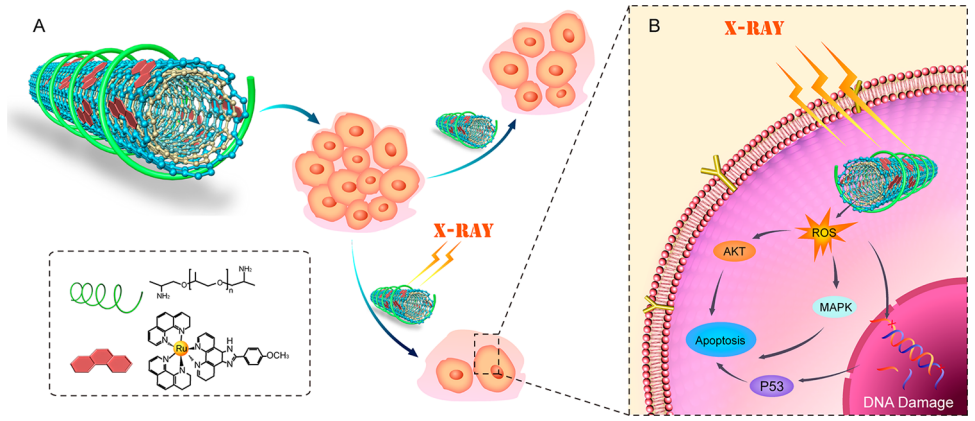

Figure 1. Rational design and radiosensitization action mechanisms of the nanosystem. (A) Chemical structure of RuPOP@MWCNTs and their sensitization of R-HepG2 drug-resistant cells to X-ray. (B) Proposed molecular mechanisms of RuPOP@MWCNTs toward R-HepG2 drug-resistant cells in combination with X-ray.

detached from SWCNTs inside the lysosomes, to give free drug, and eventually moved into the nucleus in this form; however, SWCNTs were detained in the lysosomes and maintained inside the cytoplasm.[23] Other anthracycline anticancer drugs, such as daunorubicin and epirubicin, have also been reported to attach to CNTs through $\pi-\pi$ stacking and performed with preferable efficiency.[24,25]

Radiotherapy, a typical method for cancer therapy, has become extensively used clinically for decades. In theory, the use of high-energy X-ray or γ-ray radiation can cause direct damage to DNA structures or create free radical decomposition inside cells.[26,27] Due to the noninvasive nature of radiotherapy, it brought less physical and mental burden toward patients compared to surgical or pharmaceutical. Nevertheless, radio-resistant types of cancer accepting high doses of radiation can develop to a secondary tumor and also cause damage to normal cells.[28,29] To improve the radio sensitivity and reduce the side effects, the combination of chemotherapy and radiotherapy has become a standard treatment option. There are reports about biological effects of field emission-type X-rays produced by nanomaterial.[30] The physical properties of multiwalled CNTs (MWCNTs) make them attractive carriers applied as non-invasive mediators of photothermal cancer ablation.[31,32] Researchers have demonstrated that MWCNTs exhibited heating capacities after near-infrared (NIR) irradiation, which could lead to the ablation of kidney cancer *in vitro* and *in vivo*.[33] Wang et al. reported that CNT field emission technology could develop an innovated imaging-guided micro-RT irradiation system.[34] These results have demonstrated the application potential of CNT nanosystems in cancer radiotherapy.

Ruthenium (Ru) exhibits several superior properties conducive to drug design and medicinal application, such as the suitable coordination number and low toxicity toward normal cells.[35,36] Previously, we have found that RuPOP ($[Ru(phen)_2p\text{-}MOPIP](PF_6)_2{\cdot}2H_2O$), an effective Ru polypyridyl complex with novel anticancer efficacy superior to cisplatin, could target mitochondria to induce cancer cell apoptosis.[37] However, the poor water solubility of RuPOP limited its further development and application. Thus, it shows great significance to introduce delivery systems to improve the hydrophilicity of RuPOP. Since CNTs have the ability to deliver anthracyclines into cancer cells by means of $\pi-\pi$ interaction, CNTs are eminent nanocarriers for RuPOP. Therefore, in this study, as shown in Figure 1, a CNT-based radiosensitive nanodrug delivery system was rationally designed to encapsulate RuPOP to antagonize the multidrug resistance in hepatocellular carcinoma. The functionalized nanosystem (RuPOP@MWCNTs) enhanced the cellular uptake and anticancer efficacy of RuPOP in liver cancer cells, especially drug-resistant R-HepG2 cells, but not in normal cells. This selectivity may be, at least partly, due to the positive charge of the nanosystem.[38] Interestingly, RuPOP@MWCNTs significantly enhanced the anticancer efficacy of clinically used X-ray against R-HepG2 cells through regulation of various ROS-mediated signaling pathways. Moreover, the nanosystem also effectively reduces the toxic side effects of loaded drugs and prolongs the blood circulation *in vivo*. Taken together, the results demonstrate the rational design of functionalized carbon nanotubes and their application as effective nanomedicine to overcome cancer multidrug resistance.

EXPERIMENTAL METHODS

Materials. Multiwalled carbon nanotubes (MWCNTs) were purchased from Shenzhen Nanotech Port Co. Ltd., China. Jeffamine ED 2003, 1-ethyl-3-(3-(dimethylamino)propyl) carbodiimide hydrochloride (EDC), *N*-hydroxysuccinimide (NHS), thiazolyl blue tetrazolium bromide (MTT), and dihydroethidium (DHE) were purchased from Sigma-Aldrich. Caspase substrates were purchased from Calbiology, and other chemicals used in this study are all of analytical grade. RuPOP was synthesized by our research group members. Milli-Q water used in this work was collected from an ultrapure water purification system (Millipore).

Preparation of RuPOP@MWCNTs. First, 400 mg of raw MWCNTs was treated in 100 mL of mixed H_2SO_4 and HNO_3 (1:3, v/v) solution at 80 °C in a water bath for 24 h and diluted with Milli-Q water. Then the resulting mixture was centrifuged at 10 000 rpm/min for 4−6 times to remove extra acid. The precipitate was collected and lyophilized, and then MWCNT-COOH was acquired.

In order to further enhance the water solubility of MWCNTs and prolong the circulation time *in vivo*, our study introduced the polymer with an amino group (Jeffamine ED 2003 M = 1900) on the side wall. In our study, 40 mg of MWCNTs-COOH was treated in PBS, ultrasonic to disperse completely. EDC/NHS and 100 mg of Jeffamine ED were added, and then the reaction was stirred under 96 h at 25 °C. After that, the resulting mixture was dialyzed in distilled water for 48 h (MW cutoff = 5000−8000 Da) and freeze-dried to obtain MWCNTs-NH_2.

To obtain RuPOP@MWCNT particles, 10 mg of MWCNTs-NH_2 was added to 10 mL of ethanol, ultrasonic to disperse completely. Then 10 mg of RuPOP was added to the solution and stirred for 48 h

DOI: 10.1021/acsami.5b03739
ACS Appl. Mater. Interfaces 2015, 7, 14933−14945

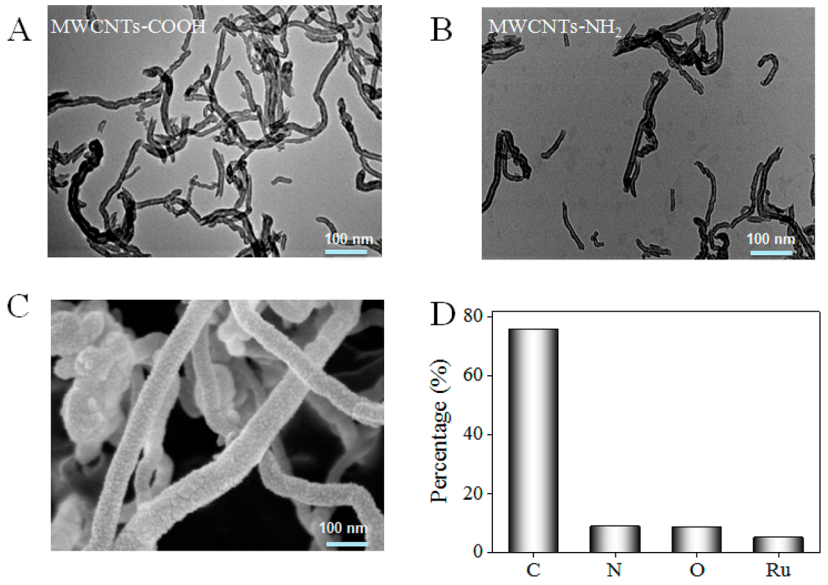

Figure 2. Morphology and structure characterizations of RuPOP@MWCNTs. TEM images of MWCNTs-COOH (A) and MWCNTs-NH_2 (B). (C) SEM image of MWCNTs-NH_2. (D) Representative results of chemical composition analysis of RuPOP@MWCNTs by EDX analysis.

at 25 °C. The product was then washed with ethanol and centrifuged. RuPOP@MWCNT was finally gathered by vacuum drying.

Labeling of RuPOP@MWCNTs by FITC. The reaction solution should be prepared with $NaHCO_3$ (7.56 g), Na_2CO_3 (1.06 g), and NaCl (7.36 g) and added to 1 L of water. An amount of 20 mg of RuPOP@MWCNTs was added to the 25 mL reaction solution. The reaction was ultrasonicated, and FITC (1 mg/mL, DMSO) was added drop by drop, then reacted for 6 h in the dark. After the reaction, the mixture was dialyzed against distilled water for 48 h (MW cutoff = 10 000 Da), and then RuPOP@MWCNT/FITC was obtained.

Characterization of RuPOP@MWCNTs. The sizes and morphologies of RuPOP@MWCNTs were monitored by transmission electron microscopy (TEM, Hitachi H-7650), scanning electron microscopy (SEM, Horiba), and zetasizer particle size analysis (Malvern Instruments Limited). The structure of RuPOP@MWCNTs was characterized by Fourier transform infrared spectroscopy (FT-IR, Equinox 55), UV−vis spectrophotometer (Carry 5000), and fluorescence spectroscopy.

***In Vitro* Drug Release of RuPOP@MWCNTs.** In brief, 5 mg of RuPOP@MWCNTs was dispersed in 5 mL of PBS at pH 7.4 and 5.3 with persistent shaking at 37 °C. After the intervals, 0.3 mL of supernatant was removed, and the same amount of PBS was added. All samples were tested for the concentration of Ru using ICP-AES.[39]

Cell Culture, MTT Assay, and Drug Treatments. Human cancer cell lines, including multidrug-resistant hepatocellular carcinoma cell lines (R-HepG2), hepatocellular carcinoma cell lines (HepG2), and hepatocyte lines (L02), were purchased from American Type Culture Collection (ATCC, Manassas, VA). The cells were maintained in Dulbecco's modified Eagle medium (DMEM) with 10% fetal bovine serum, 100 units/mL of penicillin plus 50 units/mL of streptomycin at 37 °C in a CO_2 incubator (95% relative humidity, 5% CO_2). Cell viability was measured by an MTT assay.[40] All the drug concentrations used in this study were calculated by RuPOP using ICP-AES analysis.[39]

***In Vitro* Cellular Uptake of RuPOP@MWCNTs.** The cellular uptake was analyzed by dealing with the same dose of RuPOP@MWCNTs against HepG2, R-HepG2, and L02. Briefly, the cells were seeded in 6 cm dishes and incubated for 24 h. The same dose of RuPOP@MWCNTs was added. After different intervals, cells were collected by digesting with trypsin. All samples were tested for the concentration of Ru using ICP-AES as in our previous study.[39]

Flow Cytometry Analysis. The effects of the nanomaterials on the cell cycle distribution were examined by flow cytometric analysis.[41] The percentages of cells in G0/G1, S, and G2/M phases were expressed as DNA histograms. Apoptotic cells were measured by quantifying the sub-G1 peak with hypodiploid DNA content in the cell cycle pattern.

Measurement of Intracellular Reactive Oxygen Species (ROS) Generation. Induction of ROS overproduction by RuPOP@MWCNTs was measured by the fluorescence DHE assay, which determined the fluorescence intensity of the DHE probe by using a microplate reader with the ex/em wavelengths set at 300 and 610 nm, respectively.[42]

Western Blot Analysis. Western blot analysis was employed to examine the effects of RuPOP@MWCNTs on the expression of signaling proteins in treated cells.[43]

***In Vivo* Pharmacokinetic Assay.** To investigate the effect of RuPOP@MWCNTs in blood circulation, pharmacokinetic assay was used as previously described.[22] Sprague−Dawley (SD) mice (about 140−160 g) used in this study were obtained from the Medical Laboratory Animal Center of Guangdong provice. Six mice were randomly divided into two groups, and they were fasted overnight before the experiment. The dose of RuPOP and RuPOP@MWCNTs was 3.0 mg kg^{-1} of mouse body weight (n = 3, per group) through intravenous injection. The blood samples were obtained at different time points (0, 0.5, 1, 2, 4, 8, 12, 24, 48, and 72 h). RuPOP was extracted by dissolving blood samples in HCl (0.75 M)/isopropanol at −20 °C overnight. Then, the samples were centrifuged at 12 000 rpm for 20 min, and the amount of RuPOP in the plasma was evaluated by fluorescence intensity of RuPOP, which was determined by a microplate reader with the ex/em wavelengths set at 479 and 599 nm, respectively. The plasma clearance (Cl) and the area under the blood concentration curve (AUC), which were the main pharmacokinetic parameters, were calculated using WinNonlin 3.3 software.

Biodistribution Study and Hematology Analysis. The mice were fed with RuPOP and RuPOP@MWCNTs at a dosage of 3.0 mg kg^{-1} of mouse body weight (n = 3, per group) through intravenous administration and then sacrificed at 72 h, and the organs including heart, liver, spleen, lung, and kidney were obtained. Meanwhile, the blood sample (72 h) was used for hematology analysis at Guangzhou Overseas Chinese Hospital. The drug concentration of the Ru complex in each organ was determined by fluorescence intensity, as described above.

Statistical and Synergy Analysis. All the experiments in this study were repeated at least 3 times, and the results were expressed as mean ± SD. A two-tailed Students' t test was used to analyze the difference between two groups. The difference with $P < 0.05$ (*) or $P < 0.01$ (**) was considered significant.

DOI: 10.1021/acsami.5b03739
ACS Appl. Mater. Interfaces 2015, 7, 14933−14945

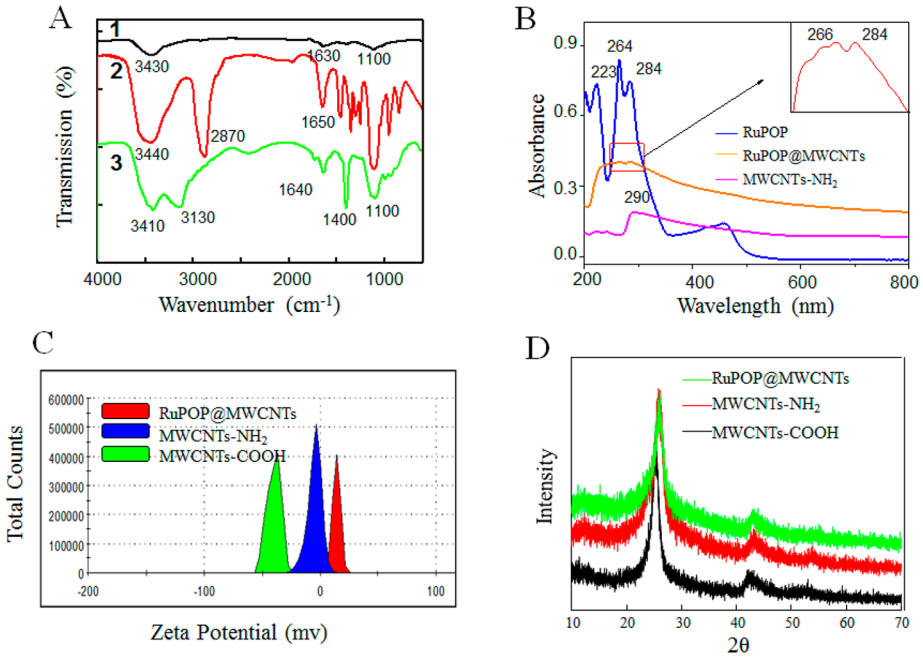

Figure 3. Structural characterization of drug loading in RuPOP@MWCNTs. (A) FTIR of MWCNTs-COOH (1), Jeffamine (2), and MWCNTs-NH_2 (3). (B) UV spectra. (C) Zeta potential analysis. (D) XRD analysis.

RESULTS AND DISCUSSION

Rational Design, Preparation, and Characterization of RuPOP@MWCNTs. Basically, the biological effects of CNTs could be affected by many factors, including metal impurities, the length, morphology, surface decoration, and dispersion.[44] Among them, metallic catalysts are regarded as the primary cause of cytotoxicity in CNTs.[45] Therefore, CNTs should be purified to remove all kinds of impurities via treating with mixed acid before biological use. Meanwhile, the carboxyl groups could be introduced to CNTs to increase their dispersity in aqueous solution and biocompatibility. In this study, we have modified MWCNTs with Jeffamine ED 2003 (block polymer with primary amine) and encapsulated RuPOP into the MWCNTs-NH_2, expecting to attain sustained release of entrapped RuPOP and the improvement of cytotoxicity to tumor cells. As shown in Figure 2A and 2B, MWCNTs-NH_2 was better dispersed compared to the TEM image of MWCNTs-COOH. The average diameter of MWCNTs-NH_2 was found at 224.9 nm (Figure S1, Supporting Information). In the results of SEM-EDX analysis, the presence of the Ru signal revealed the successful loading of RuPOP into the nanosystem (Figure 2C,D and Figure S2, Supporting Information). FT-IR was also used to confirm the formation process of the nanosystem. In Figure 3A, the peak at 1640 cm^{-1} in MWCNTs-NH_2 was assigned to amino groups. Compared with MWCNTs, MWCNTs-NH_2 displayed three special peaks at 3130, 2420, and 1728 cm^{-1}. These results indicated that Jeffamine ED 2003 has been successfully conjugated to oxidized MWCNTs via amino linkage. Furthermore, the UV−vis spectrum of RuPOP@MWCNTs displayed specific peaks from RuPOP, which comfirmed the successful loading of RuPOP (Figure 3B). Zeta potential is also used to characterize the changes in surface properties of the nanosystem. As shown in Figure 3C, the zeta potential of MWCNTs-COOH was −37 mV. However, after conjugation of Jeffamine ED and loading of RuPOP, the zeta potential was further increased to +2.3 and +24.3 mV. The difference in zeta potential demonstrated the absorption of RuPOP to MWCNTs. Figure 3D shows that no peak shifted among RuPOP, RuPOP@MWCNTs, and MWCNTs-NH_2 in the analysis of XRD, and the characteristic peak of CNTs remained 25.3°, which demonstrated that the drug loading did not alter the crystalline structure of MWCNTs. Moreover, the solubility of the free drug RuPOP was found at 14.8 μg/mL in water. However, after loading with MWCNTs-NH_2, the solubility was significantly improved. For instance, 1 mg of RuPOP@MWCNTs (with 98 μg of RuPOP/mg) could be well dispered in 1 mL of water, which is about 6.59-fold higher than that of free RuPOP.

XPS was used to illustrate the surface structure and interaction between MWCNTs and drug based on the chemical and electronic state. The presence of a characteristic peak of Ru in the spectrum of RuPOP@MWCNTs confirmed the loading of RuPOP into the nanomaterials (Figure 4A). Moreover, the changes in C 1s and N 1s spectra of RuPOP, MWCNTs-NH_2, and RuPOP@MWCNTs were analyzed to examine their interactions. The increase in the binding energy of C 1s in MWCNTs-NH_2 after drug loading suggests that RuPOP could be adsorbed to the surface of MWCNTs-NH_2 by $\pi-\pi$ stacking (Figure 4B). Meanwhile, the decrease in the N 1s binding energy of MWCNTs-NH_2 suggests the formation of a hydrogen bond between RuPOP and the amino groups on the surface of MWCNTs (Figure 4C). Moreover, as determined by ICP-AES, the loading efficiency and encapsulation efficiency of RuPOP@MWCNTs were found at 9.8% and 19.7%, respectively. Taken together, these results supported the successful construction of RuPOP@MWCNT, a novel CNT-based nanomedicine.

In Vitro Anticancer Activity of RuPOP@MWCNTs. This study aimed to construct and develop MWCNTs-NH_2 as a carrier of RuPOP to overcome its shortcomings of low solubility and low cell membrane penetrating ability. Therefore, we have compared the effects of RuPOP@MWCNTs on a series of cancer cells by MTT assay with the free RuPOP. As shown in Figure 5A, RuPOP@MWCNTs exhibited anticancer

DOI: 10.1021/acsami.5b03739
ACS Appl. Mater. Interfaces 2015, 7, 14933−14945

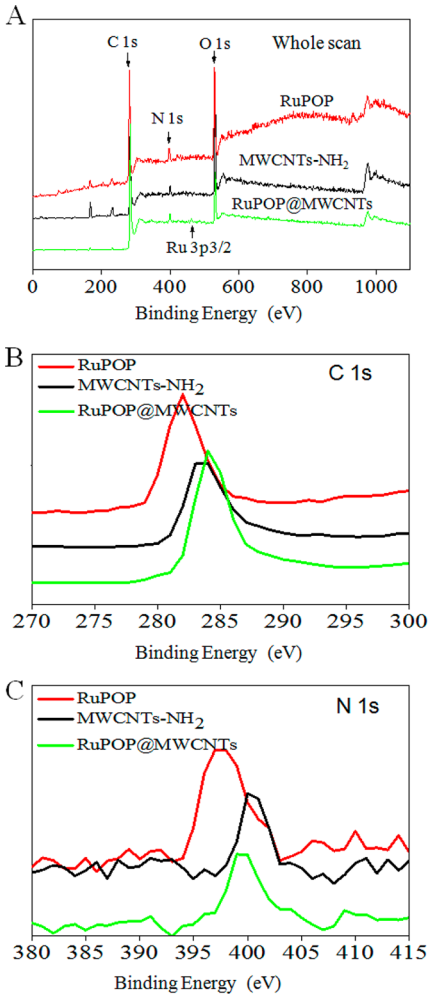

Figure 4. XPS characterization of RuPOP@MWCNTs. (A) XPS spectra of RuPOP, MWCNTs-NH_2, and RuPOP@MWCNTs. (B) Binding energy of C 1s spectra. (C) Binding energy of N 1s spectra.

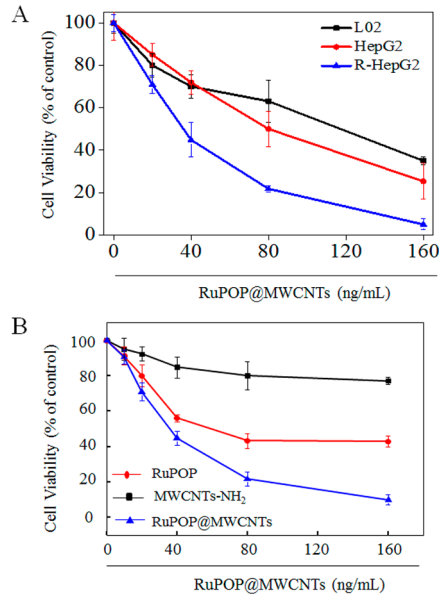

Figure 5. Anticancer activity and selectivity of the nanosystem. The drug concentration was calculated as RuPOP. (A) Cell viability was examined by MTT assay (72 h). (B) Viability of R-HepG2 treated for 72 h. All results were obtained from three independent experiments.

effects against HepG2 and R-HepG2 cells in a dose-dependent manner, especially for R-HepG2. The IC_{50} values of RuPOP@MWCNTs on R-HepG2 and HepG2 cells were 40 and 100 ng/mL, respectively. Interestingly, an equal dose of RuPOP@MWCNTs showed much lower cytotoxicity toward L02 normal liver cells. In order to exclude the cytotoxic effects of MWCNTs-NH_2, R-HepG2 cells were treated with RuPOP, MWCNTs-NH_2, and RuPOP@MWCNTs, and the cellular viability was detected by MTT assay. As shown in Figure 5B, MWCNTs-NH_2 only slightly inhibited the cancer cell growth. Even at the concentration of 160 ng/mL, the cell viability was still over 80%. Moreover, in the concentrations of 40−160 ng/mL, the free RuPOP exhibited much lower growth inhibition on R-HepG2 cells than RuPOP@MWCNTs. Meanwhile, as shown in Figure S3 (Supporting Information), MWCNTs-NH_2 alone demonstrated low cytotoxicity against HepG2 and L02 cells. Taken together, these results indicated that the functionalized MWCNT nanosystem effectively enhances the anticancer efficacy of RuPOP.

Endocytosis of RuPOP@MWCNTs and pH-Mediated Drug Release. Cellular uptake efficacy is an important contributor to the biological action of anticancer nanomedicine.[19] Therefore, to control and enhance the selective cellular uptake of nanomedicine in cancer cells is a good strategy for rational design of new cancer therapeutics. To verify the selectivity of RuPOP@MWCNTs between cancer and normal cells, we further studied the cellular uptake of RuPOP@MWCNTs in R-HepG2, HepG2, and L02 cells by determining the intracellular Ru content by ICP-AES analysis. As shown in Figure 6A, the amount of intracellular drug accumulated in the cells significantly in a time-dependent manner. Meanwhile, the data revealed that the cellular uptake of RuPOP@MWCNTs in R-HepG2 cells was higher than in HepG2 and L02 cells after incubation for 2, 4, and 6 h. More importantly, the cellular uptake in L02 cells was about 1−2 times lower than those in R-HepG2 and HepG2 cells. The results suggest that RuPOP@MWCNTs exhibit good selectivity between human cancer and normal cells. Consistently, our previous study has found that nanoparticles with higher positive charge exhibited stronger affinity for the negatively charged cancer cell membrane, thus accounting for higher cellular uptake and anticancer activities.[38] Therefore, the selective cellular uptake and the anticancer action of RuPOP@MWCNTs may be, at least partly, due to the positive charge of the nanosystem.

Furthermore, the localization of RuPOP@MWCNTs/FITC was studied by using Lyso-Tracker (red) to label lysosomes and DAPI to label the nucleus. As shown in Figure 6B, the good merging of the green and red fluorescence clearly demonstrated the colocalization of RuPOP@MWCNTs/FITC and lysosomes, indicating RuPOP@MWCNTs/FITC penetrate the cells through endocytosis via lysosomes. In the detailed time-dependent analysis, we discovered that RuPOP@MWCNTs/FITC aggregated around the membranes after 2 h. In the course of time, the green fluorescence became stronger, which indicated nanotubes could enter into cancer cells by the transportation of lysosomes. In addition, we studied drug release of RuPOP@MWCNTs in PBS with different pH values to simulate the environments of body fluids and lysosomes. From the results of Figure 6C, RuPOP was released faster under the acidic solution (pH 5.3) than that at pH 7.4. Due to

DOI: 10.1021/acsami.5b03739
ACS Appl. Mater. Interfaces 2015, 7, 14933−14945

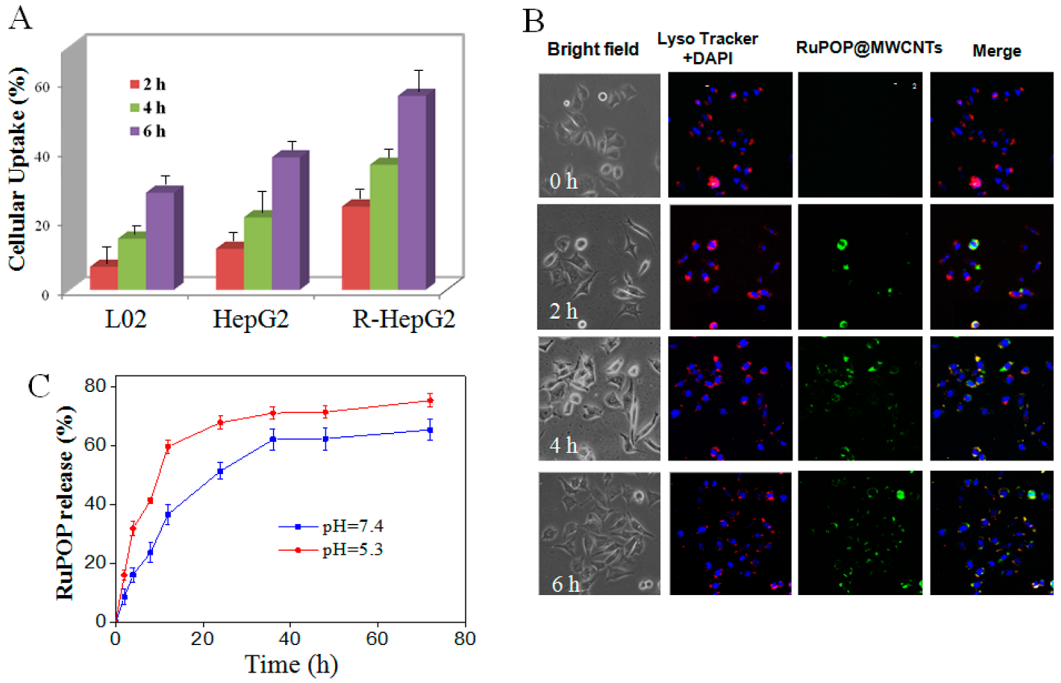

Figure 6. Cellular uptake, intracellular localization, and drug release of RuPOP@MWCNTs. (A) Quantitative analysis of cellular uptake efficiency of RuPOP@MWCNTs (160 ng/mL) in various cancer and normal cells after different time periods of incubation. (B) Colocalization of RuPOP@MWCNTs/FITC (green fluorescence) and lysosomes (red fluorescence) in cancer cells. (C) *In vitro* release profiles of RuPOP from RuPOP@MWCNTs in PBS solution (pH 7.4 and pH 5.3). The Ru concentration was determined by ICP-AES.

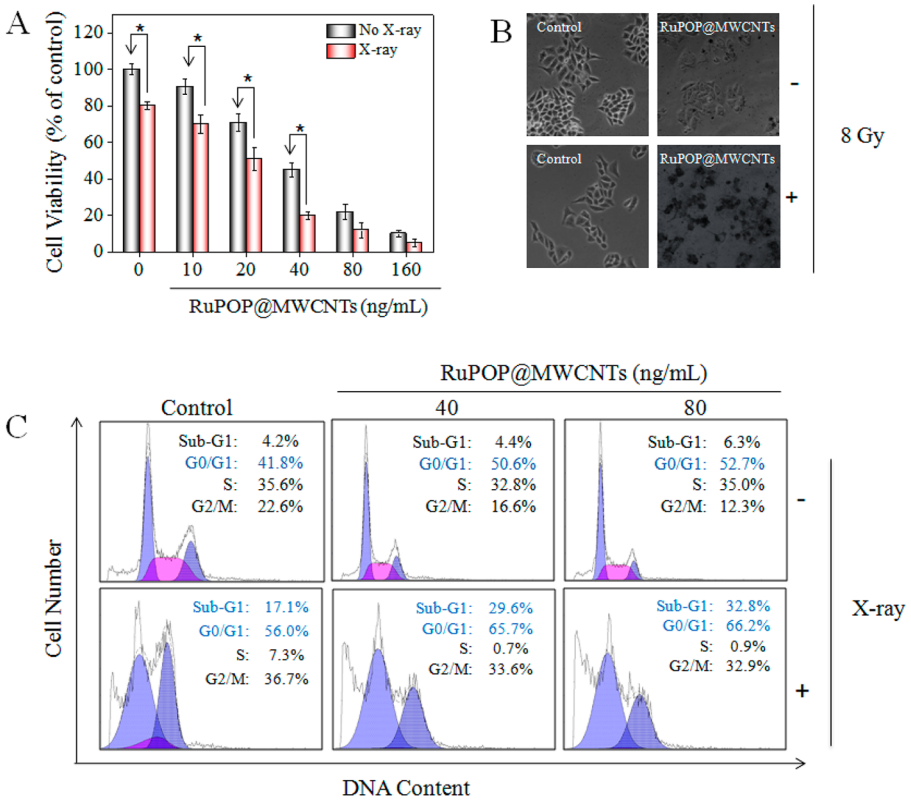

Figure 7. Radiosensitization effects of RuPOP@MWCNTs on X-ray (8 Gy). (A) Viability of R-HepG2 cells treated with RuPOP@MWCNTs with and without X-ray as examined by MTT assay (24 h). (B) Morphology of R-HepG2 cells under different treatments. (C) Flow cytometry analysis of R-HepG2 exposed to RuPOP@MWCNTs for 24 h with (+) and without (−) X-ray treatment. The differences were analyzed by X-ray and no X-ray groups, and those with $P < 0.05$ (*) or $P < 0.01$ (**) were considered significant.

the protonation of the amino groups on the surface of MWCNTs under acidic solution (pH 5.3), RuPOP could be replaced by protonation, and then RuPOP released into the solution, which eventually led to faster and higher drug release.

DOI: 10.1021/acsami.5b03739
ACS Appl. Mater. Interfaces 2015, 7, 14933−14945

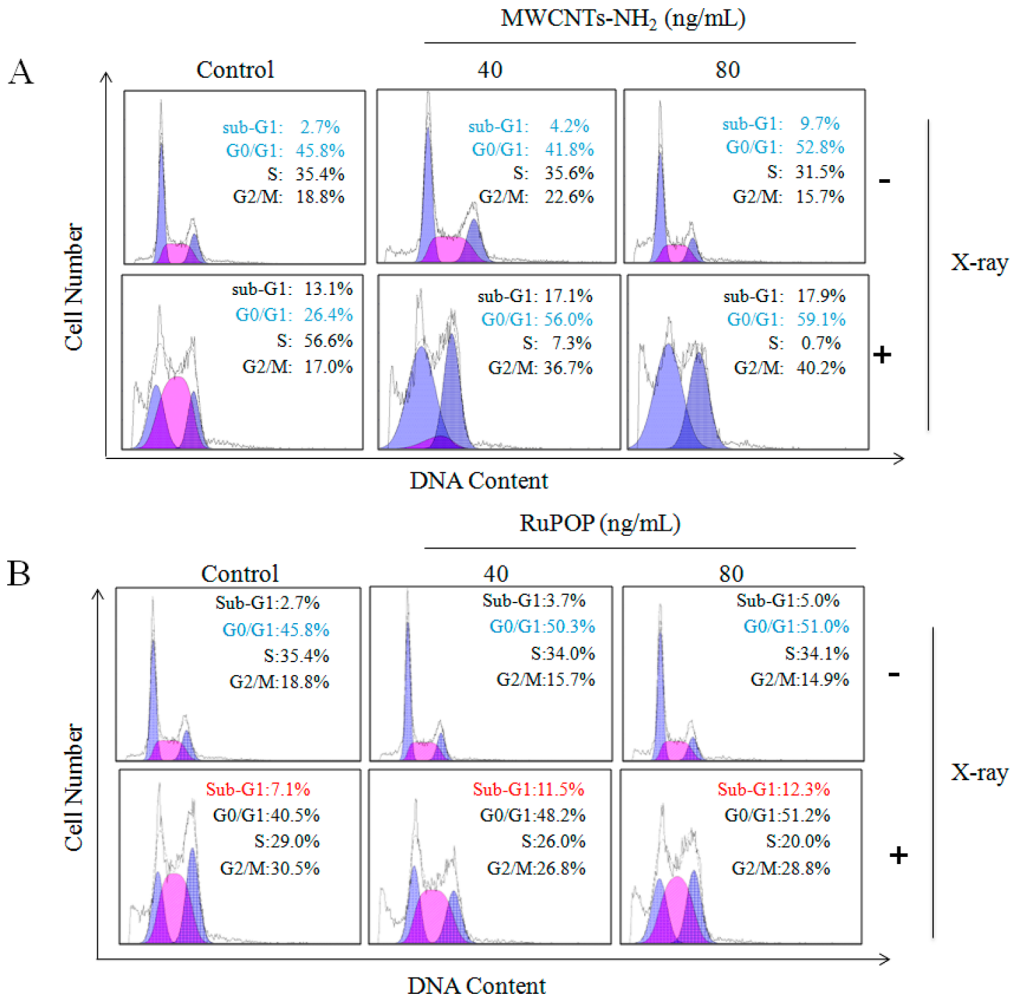

Figure 8. Radiosensitization effects of MWCNTs-NH_2 (A) and RuPOP (B) in combination with X-ray (8 Gy), and their effects on the cell cycle distribution of R-HepG2 cells were examined by flow cytometry analysis (24 h).

These outcomes also illustrated that the RuPOP@MWCNTs could achieve faster release in the lysosomes.

RuPOP@MWCNTs Sensitize R-HepG2 Cell Radiotherapy. Most liver cancer patients with liver cirrhosis and hepatic insufficiency have difficulty in successful clinical treatments.[46,47] Recently, comprehensive treatment of liver cancer has achieved better and better clinical efficacy. The inhibition rates of tumor growth and patient survival time have increased after comprehensive chemoradiotherapy.[48−50] Therefore, radiotherapy plays an increasingly important role in the treatment of liver cancers.[51] In this study, we found that RuPOP@MWCNTs could enhance the sensitivity of R-HepG2 cells to X-ray. As shown in Figure 7A, R-HepG2 cells were treated with RuPOP@MWCNTs (10−160 ng/mL) for 2 h and then treated with 8 Gy X-ray radiation and incubated for another 24 h. The cell viability of R-HepG2 cells was determined by MTT assay. RuPOP@MWCNTs performed a dose-dependent effect against R-HepG2 cells regardless of radiation. However, RuPOP@MWCNTs combined with X-ray radiation significantly enhanced the anticancer activity in R-HepG2 cells compared to the group without radiation. For instance, at the concentration of 40 ng/mL, the cell viability of the radiation group declined to 20%, while the group without radiation was 44.8%. In addition, we took the picture of morphology of R-HepG2 cells with and without radiation. From Figure 7B, we clearly found that even though the radiotherapy has a certain degree of growth inhibition, it did not lead to obvious cell death. Nevertheless, RuPOP@MWCNTs combined with X-ray caused a large number of cell deaths at a low concentration (40 ng/mL). Additionally, the cell growth was restrained with RuPOP@MWCNTs alone, yet the cell morphology did not change and did not cause obvious cell death. These results preliminarily indicated that RuPOP@MWCNTs could enhance the efficiency of radiotherapy in R-HepG2 cells.

Apoptosis is a process of programmed cell death (PCD) that may occur in multicellular organisms.[52] Biochemical events lead to characteristic cell changes (morphology) and death. These changes include blebbing, cell shrinkage, nuclear fragmentation, chromatin condensation, and chromosomal DNA fragmentation. To verify whether apoptosis was involved in cell death triggered by RuPOP@MWCNT combination with and without radiation, further investigation with flow cytometry was carried out toward R-HepG2 cells. As shown in Figure 7C, we have found that RuPOP@MWCNTs combined with X-ray treatments could significantly induce cancer cell apoptosis and G0/G1 phase arrest. Before radiotherapy, RuPOP@MWCNTs mainly inhibited cells in G0/G1 phase growth. At the concentration of 80 ng/mL, the percentage of G0/G1 peaks was 52.7%, which was higher than the control group (41.8%). After radiotherapy, at the concentration of 80 ng/mL, the

DOI: 10.1021/acsami.5b03739
ACS Appl. Mater. Interfaces 2015, 7, 14933−14945

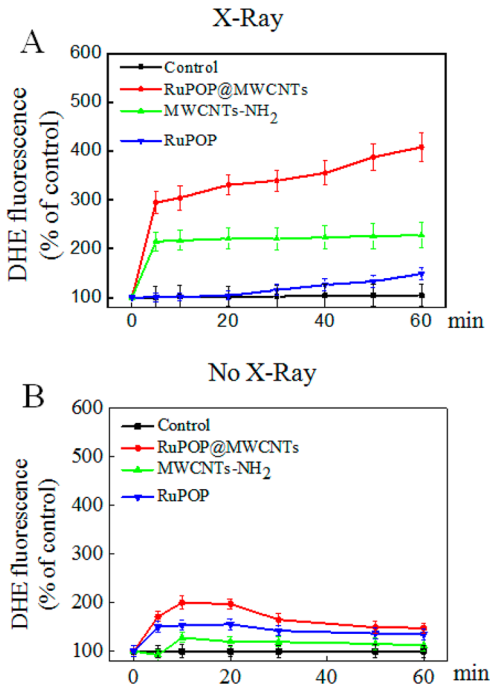

Figure 9. Activation of intracellular ROS generation by RuPOP@MWCNTs (160 ng/mL), MWCNTs-NH_2 (equal amount), and RuPOP (160 ng/mL) in R-HepG2 cells with (A) and without (B) X-ray. The intracellular ROS level was determined by measuring the fluorescent intensity of DHE.

percentage of sub-G1 increased to 32.8% from 17.1% (control). Meanwhile, the cell population of G0/G1 peaks was 66.2%, which was higher than the control group (56.0%). We further analyzed the effects of RuPOP and MWCNTs-NH_2 on the cell cycle distribution of R-HepG2 cells by flow cytometry analysis. As shown in Figure 8, RuPOP and MWCNTs-NH_2 demonstrated slight enhancement on the anticancer action of radiotherapy. For instance, MWCNTs-NH_2 alone displayed no cytotoxicity but induced obvious cell apoptosis by combination with radiotherapy. These results indicated that RuPOP@MWCNTs potentiated X-ray-induced growth inhibition on R-HepG2 cells by triggering apoptosis and G0/G1 cell cycle arrest.

RuPOP@MWCNT Enhanced Cell Apoptosis via Activating ROS Generation. Intracellular ROS are important chemical signal molecules regulating signal transduction activated by multifarious anticancer drugs, such as cisplatin and Ru complexes.[53,54] Generally, excessive ROS generation could react with proteins and DNA inside the cells, resulting in protein modification and DNA damage and then triggering cell death via regulation of different downstream signaling pathways. In order to examine the roles of ROS in cell apoptosis, R-HepG2 cells were exposed to RuPOP@MWCNTs (160 ng/mL), RuPOP (160 ng/mL), and MWCNTs-NH_2 (equal amount), and then the cellular ROS levels were measured by the DHE fluorescence method. It can clearly be seen from Figure 9 that RuPOP@MWCNTs, RuPOP, and MWCNTs-NH_2 could cause ROS overproduction in a different degree, especially RuPOP@MWCNTs. Before radiotherapy, the rise of intracellular ROS levels remains below 200% (Figure 9B). For instance, we observed that RuPOP@MWCNTs elevate ROS generation (199.9%), which was higher than that treated with RuPOP (153.1%) and MWCNTs-NH_2 (127.7%) at 10 min. Interestingly, after radiotherapy, intracellular ROS levels with RuPOP@MWCNTs increased to above 300%, and intracellular ROS levels with MWCNTs-NH_2 were much higher than the MWCNTs-NH_2 without X-ray (Figure 9A). Specifically, after radiotherapy, RuPOP@MWCNTs elevate ROS production (303.9%), which was higher than treated with RuPOP (100.2%) and MWCNTs-NH_2 (214.9%) at 10 min. Those outcomes indicated that RuPOP@MWCNTs triggered a higher ROS level than RuPOP and MWCNTs-NH_2. More importantly, RuPOP@MWCNTs combined with radiotherapy could significantly cause ROS overproduction contrast to the group without X-ray, which was consistent with the results of flow cytometry.

RuPOP@MWCNT Triggers Caspase Activation and Mitochondria Dysfunction by Regulating Bcl-2 Family Proteins. Caspases are aware of playing essential roles in

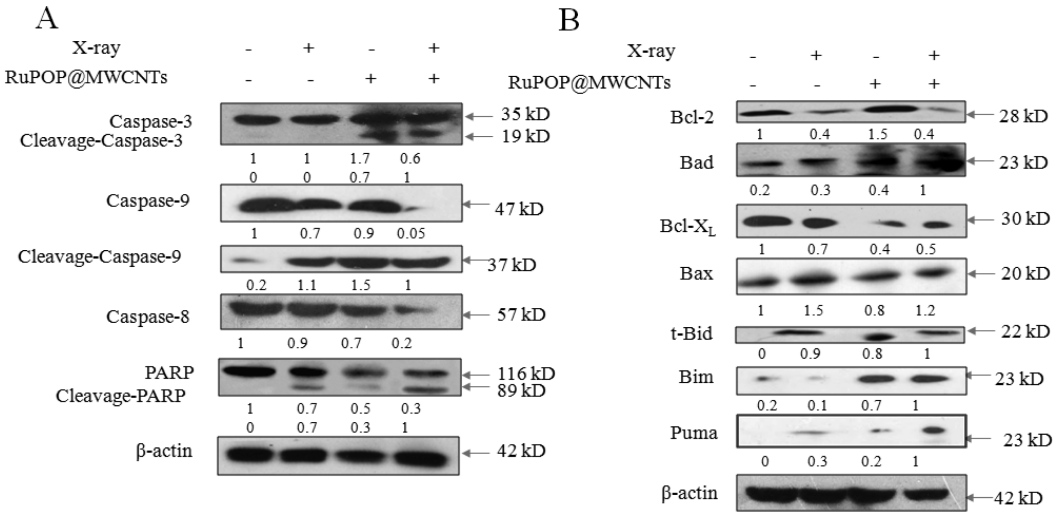

Figure 10. Activation of apoptotic pathways by combined treatment of RuPOP@MWCNTs and X-ray. (A) Western blot analysis of the quantitative of PARP and caspases cleaved in the apoptosis induced by RuPOP@MWCNTs (80 ng/mL) with (+) and without (−) X-ray (8 Gy) treatment. (B) Western blot analysis of the expression levels of Bad, Bcl-X_L, Bax, Bcl-2, t-Bid, Bim, and Puma in R-HepG2 cells treated by RuPOP@MWCNTs (80 ng/mL) with (+) and without (−) X-ray treatment. The protein expression was determined by Quantity One Software.

DOI: 10.1021/acsami.5b03739
ACS Appl. Mater. Interfaces 2015, 7, 14933−14945

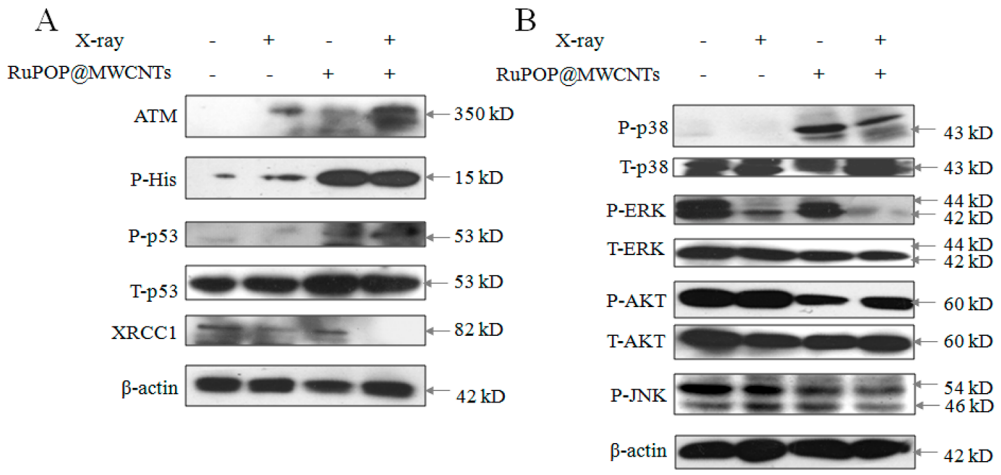

Figure 11. Activation of ROS-mediated apoptotic signaling pathways by RuPOP@MWCNTs and X-ray. (A) RuPOP@MWCNT (80 ng/mL) enhances radiation-induced (8 Gy) apoptosis by triggering p53 phosphorylation. (B) Effects of radiation and RuPOP@MWCNTs (80 ng/mL) on AKT and MAPK pathways.

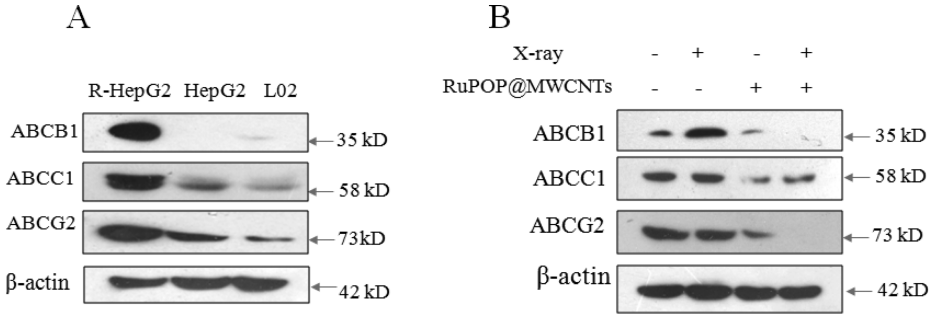

Figure 12. (A) Difference in expression levels of ABC family proteins in R-HepG2, HepG2, and L02 cells. (B) Effects of RuPOP@MWCNTs combined with or without X-ray on expression levels of ABC family in R-HepG2 cells.

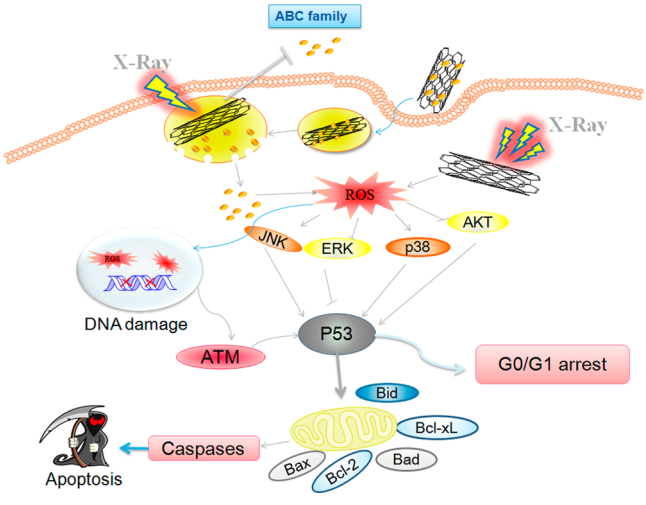

Figure 13. Proposed signaling pathways accounting for cell apoptosis and G0/G1 cell cycle arrest triggered by RuPOP@MWCNTs in combination with radiotherapy.

apoptosis (programmed cell death) and conducive to the overall morphology of apoptosis via cleavage of caspase substrates. In this study, we have examined the activation of caspases, the cleavage of caspases, and PARP by Western blotting. From Figure 10A, exposure of R-HepG2 cells to the treatment of RuPOP@MWCNTs or radiotherapy alone led to a slight cleavage of caspases-3/8/9. In addition, the combined treatment of RuPOP@MWCNTs and radiotherapy synergistically enhanced the decrease of total caspase-3/8/9 and increase of cleaved caspase-3/9. The activation of caspase-3 subsequently triggered the PARP cleavage, an important biochemical hallmark of cell apoptosis. Furthermore, we also measured the caspase-3 activity in R-HepG2 cells treated with RuPOP@MWCNTs with or without X-ray, and the results revealed that the combined treatments significantly enhanced the caspase-3 activation in cancer cells (Figure S4, Supporting Information), which was consistent with the results of Western blotting. Overall, these results indicate that the combined treatment induced apoptosis in R-HepG2 cells through activation of both the extrinsic and intrinsic apoptosis pathways.

Apoptosis regulator Bcl-2 is a family of evolutionarily related proteins, which governs the mitochondria-mediated apoptosis pathway. Hence we monitored the effects of RuPOP@MWCNTs and radiotherapy on the expression levels of proapoptotic and antiapoptotic Bcl-2 family proteins in R-HepG2 cells via Western blotting. As shown in Figure 10B, RuPOP@MWCNTs and radiotherapy increased the overall expression levels of the pro-apoptotic proteins, such as Bad, Bax, Bim, and Puma but decreased the expression levels of antiapoptotic proteins (Bcl-X_L and Bcl-2). Truncation of Bid (tBid), an activated form of Bid that exhibits potent proapoptotic activity, was significantly improved. Taken together, the activation of caspase-9 and regulation of Bcl-2 family proteins indicates that the enhancement of radiotherapy-

DOI: 10.1021/acsami.5b03739
ACS Appl. Mater. Interfaces 2015, 7, 14933−14945

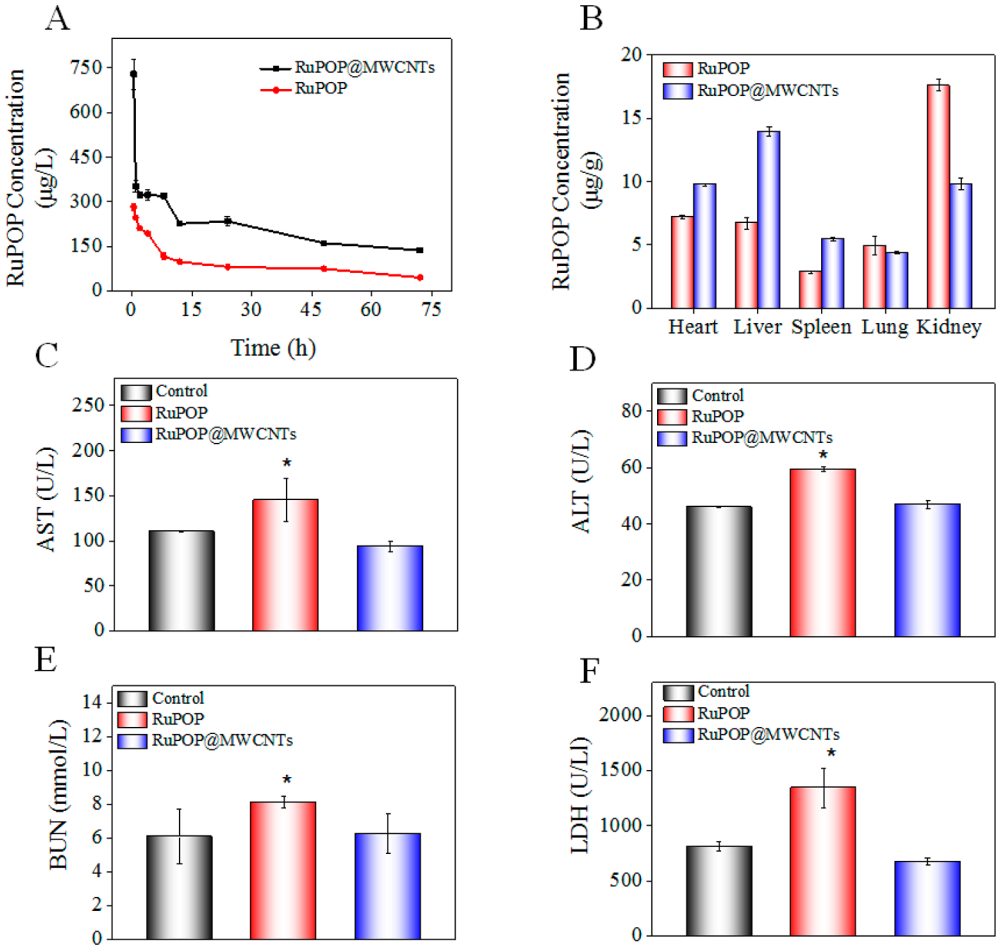

Figure 14. (A) Concentration of RuPOP in plasma at different time after intravenous injection of RuPOP and RuPOP@MWCNTs at a dose of 3.0 mg kg^{-1} calculated by RuPOP. (B) *In vivo* biodistribution of RuPOP and RuPOP@MWCNTs in major organs after intravenous injection for 72 h. Blood biochemistry analysis of mice treated with RuPOP and RuPOP@MWCNTs (72 h). The results showed as mean ± S.D. of (C) aspartate aminotransferase (AST), (D) alanine aminotransferase (ALT), (E) blood urea nitrogen (BUN), and (F) lactate dehydrogenase (LDH). The difference was analyzed between treatment and control groups, and those with $P < 0.05$ (*) or $P < 0.01$ (**) were considered significant.

induced apoptosis by RuPOP@MWCNTs involved the activation of the mitochondria-mediated apoptotic pathway.

RuPOP@MWCNTs and Radiotherapy Synergize to Induce DNA Damage Mediated p53 Phosphorylation. The regulation of the p53 has a key role toward mitochondrial-mediated apoptosis and death receptor mediated apoptosis, which is the central protein in the process of cell apoptosis. Therefore, we examined the protein level of phosphorylated p53. We found that the treatment of RuPOP@MWCNTs combined with radiotherapy induced the expression of P-p53 to significant improve along with the same protein level of total p53 (Figure 11A). ROS overproduction could cause the change toward MAPKs, including ERK, p38, MAPK, and JNK in phosphorylation and protein level. As shown in Figure 11B, phosphorylation of ERK was almost completely suppressed after treatment of RuPOP@MWCNTs combined with radiotherapy, but it only caused slight dephosphorylation with treatment of RuPOP@MWCNTs only. In addition, phosphorylated p38 increased, and p-JNK did not cause obvious changes. The results demonstrated that MAPK and AKT pathways were activated by RuPOP@MWCNTs in combination with radiotherapy.

RuPOP@MWCNTs Inhibit the Expression of ABC Family Proteins. ABC family proteins play important roles in multidrug resistance in cancers. Therefore, it is an effective strategy to antagonize cancer multidrug resistance via down-regulating the expression levels of these proteins. To verify whether ABC family proteins mediated the multidrug resistance, Western blotting was used to analyze the expression levels of these proteins. As shown in Figure 12A, the expression levels of these proteins in R-HepG2 cells were significantly higher than those in HepG2 and L02 cells. Furthermore, we examined the effects of RuPOP@MWCNTs with or without X-ray on the expression levels of the ABC family protein. As shown in Figure 12B, the results showed that the combined treatment effectively inhibited the expression levels of ABCB1, ABCC1, and ABCG2 in R-HepG2 cells. The effects were much higher than those of X-ray and RuPOP@MWCNTs alone. These results demonstrated that the RuPOP@MWCNTs could reverse cancer multidrug resistance by inhibition of ABC family proteins. On the basis of these results, the signaling pathways accounting for apoptosis induced by RuPOP@MWCNTs combined with radiotherapy were summarized in Figure 13.

Pharmacokinetics, Biodistribution, and Hematological Analysis of RuPOP@MWCNTs. To evaluate the application potential of the nanosystem *in vivo*, RuPOP@MWCNTs were injected intravenously into mice to analyze their pharmacokinetics and biodistribution and the effects on

DOI: 10.1021/acsami.5b03739
ACS Appl. Mater. Interfaces 2015, 7, 14933−14945

hematological parameters. As shown in Figure 14A, two-compartment pharmacokinetics happened in RuPOP and RuPOP@MWCNTs. The C_{max} of RuPOP@MWCNTs was 15 times that of RuPOP (Table S1, Supporting Information). Moreover, the pharmacokinetics parameters of AUC_{0-72h} in blood with RuPOP@MWCNTs increased to 25818.8 μg/L*h, which was much higher than that of free RuPOP (10241.8 μg/L*h). Furthermore, after loading into MWCNTs-NH_2, the $t_{1/2\beta}$ of RuPOP was prolonged from 55.1 h (RuPOP) to 61.6 h (RuPOP@MWCNTs). Consequently, the clearance of RuPOP@MWCNTs was decreased to 0.017 L h^{-1} from 0.044 L h^{-1} (RuPOP). These results demonstrated that the nanosystem significantly prolonged the blood circulation time of RuPOP *in vivo*. Furthermore, the mice were sacrificed after drug treatment to further investigate the biodistribution of RuPOP@MWCNTs in different organs, and the blood samples (72 h) were subjected to hematological analysis. As shown in Figure 14B, RuPOP and RuPOP@MWCNTs accumulated less in spleen and lung by comparing with other organs. Nevertheless, the accumulation of RuPOP@MWCNTs in liver increased from 6.70 μg/g (RuPOP) to 13.95 μg/g, which could be due to the reticuloen−dothelial system (RES) uptake. In addition, the accumulation of RuPOP@MWCNTs in kidney was 9.84 μg/g, which was much lower than that of RuPOP (17.6 μg/g). These data suggested that the nanosystem may be easily cleared by renal excretion.

Futhermore, the results of hematological analysis revealed that the mice treated with RuPOP showed increased levels of aspartate aminotransferase (AST), alanine amiotransferase (ALT), blood ureannitrogen (BUN), and lactate dehydrogenase (LDH) than the control group. Interestingly, RuPOP@MWCNTs at the same dose showed no significant effects on these parameters (Figure 14C−F). AST and ALT are important indicators of liver function. BUN and LDH are important indicators of kidney and heart function, respectively. Therefore, the increased levels of these parameters in the RuPOP-treated group demonstrated the possible damage in the liver, heart, and kidney. The changes in other parameters with no significant difference were summarized in Figure S5 (Supporting Information). Taken together, these results demonstrate that the functionalized MWCNT nanosystem could effectively reduce the *in vivo* toxicity of the loaded drug RuPOP, which further supports its future clinical application.

CONCLUSIONS

Multidrug resistance and radioresistance are major obstacles for successful cancer therapy. Herein, a CNT-based radiosensitive nanodrug delivery system was rationally designed to antagonize the multidrug resistance in hepatocellular carcinoma. The nanosystem was loaded with a potent anticancer Ru complex RuPOP via $\pi-\pi$ interaction and formation of hydrogen bond. The functionalized nanosystem enhanced the cellular uptake of RuPOP in liver cancer cells, especially drug-resistant R-HepG2 cells, through endocytosis. Consistently, the selective cellular uptake endowed the nanosystem amplified anticancer efficacy against R-HepG2 cells but not in normal cells. The selective cellular uptake and the anticancer action of RuPOP@MWCNTs may be, at least partly, due to the positive charge of the nanosystem. Interestingly, RuPOP@MWCNTs significantly enhanced the anticancer efficacy of clinically used X-ray against R-HepG2 cells through induction of apoptosis and G0/G1 cell cycle arrest, with the involvement of ROS overproduction, which activated several downstream signaling pathways, including DNA damage-mediated p53 phosphorylation, activation of p38, and inactivation of AKT and ERK. Moreover, the nanosystem also effectively reduces the toxic side effects of loaded drugs and prolongs the blood circulation *in vivo*. Taken together, the results demonstrate the rational design of functionalized carbon nanotubes and their application as effective nanomedicine to overcome cancer multidrug resistance.

ASSOCIATED CONTENT

Supporting Information

The size distribution of MWCNTs-NH_2 by intensity; chemical composition analysis of RuPOP@MWCNTs by EDX; the cell viability of MWCNTs-NH_2 (5−160 μg/mL) against HepG2 and L02 cells (72 h); hematology analysis of mice treated with RuPOP and RuPOP@MWCNTs (72 h); and the activity of caspase-3 in R-HepG2 cells after treatment of RuPOP@MWCNTs with or without X-ray. The Supporting Information is available free of charge on the ACS Publications website at DOI: 10.1021/acsami.5b03739.

AUTHOR INFORMATION

Corresponding Author

*E-mail: tchentf@jnu.edu.cn. Tel.: +86 20-85225962. Fax: +86 20 85221263.

Author Contributions

†These authors contributed equally to the work.

Notes

The authors declare no competing financial interest.

ACKNOWLEDGMENTS

This work was supported by National High Technology Research and Development Program of China (863 Program, SS2014AA020538), Science Foundation for Distinguished Young Scholars (S2013050014667) of Guangdong Province, Natural Science Foundation of China, Foundation for High-level Talents in Higher Education of Guangdong, Guangdong Special Support Program and Guangdong Frontier and Key Technological Innovation Special Funds.

REFERENCES

(1) Prudent, R.; Vassal-Stermann, E.; Nguyen, C. H.; Pillet, C.; Martinez, A.; Prunier, C.; Barette, C.; Soleilhac, E.; Filhol, O.; Beghin, A.; Valdameri, G.; Honore, S.; Aci-Seche, S.; Grierson, D.; Antonipillai, J.; Li, R.; Di Pietro, A.; Dumontet, C.; Braguer, D.; Florent, J. C.; Knapp, S.; Bernard, O.; Lafanechere, L. Pharmacological Inhibition of LIM Kinase Stabilizes Microtubules and Inhibits Neoplastic Growth. *Cancer Res.* **2012**, *72*, 4429−4439.

(2) Murphy, J. T.; Burey, A. P.; Beebe, A. M.; Gu, D. L.; Presta, L. G.; Merghoub, T.; Wolchok, J. D. Anaphylaxis Caused by Repetitive Doses of a GITR Agonist Monoclonal Antibody in Mice. *Blood* **2014**, *123*, 2172−2180.

(3) Li, X.; Zeng, X. L.; Sun, J. G.; Li, H.; Wu, P.; Fung, K. P.; Liu, F. Y. Imperatorin Induces Mcl-1 Degradation to Cooperatively Trigger Bax Translocation and Bak Activation to Suppress Drug-Resistant Human Hepatoma. *Cancer Lett.* **2014**, *348*, 146−155.

(4) Liu, Z.; Duan, Z. J.; Chang, J. Y.; Zhang, Z. F.; Chu, R.; Li, Y. L.; Dai, K. H.; Mo, G. Q.; Chang, Q. Y. Sinomenine Sensitizes Multidrug-Resistant Colon Cancer Cells (Caco-2) to Doxorubicin by Down-regulation of MDR-1 Expression. *PLoS One* **2014**, *9*, e98560.

(5) Sun, M.; Su, X.; Ding, B. Y.; He, X. L.; Liu, X. J.; Yu, A. H.; Lou, H. X.; Zhai, G. X. Advances in Nanotechnology-Based Delivery Systems for Curcumin. *Nanomedicine* **2012**, *7*, 1085−1100.

DOI: 10.1021/acsami.5b03739
ACS Appl. Mater. Interfaces 2015, 7, 14933−14945

(6) Sahoo, S. K.; Labhasetwar, V. Nanotech Approaches to Delivery and Imaging Drug. *Drug Discovery Today* **2003**, *8*, 1112−1120.
(7) Sharma, P.; Garg, S. Pure Drug and Polymer Based Nanotechnologies for the Improved Solubility, Stability, Bioavailability and Targeting of Anti-HIV Drugs. *Adv. Drug Delivery Rev.* **2010**, *62*, 491−502.
(8) Ma, Y.; Pan, G.; Zhang, Y.; Guo, X.; Zhang, H. Narrowly Dispersed Hydrophilic Molecularly Imprinted Polymer Nanoparticles for Efficient Molecular Recognition in Real Aqueous Samples Including River Water, Milk, and Bovine Serum. *Angew. Chem., Int. Ed.* **2013**, *52*, 1511−1514.
(9) Rana, S.; Bajaj, A.; Mout, R.; Rotello, V. M. Monolayer Coated Gold Nanoparticles for Delivery Applications. *Adv. Drug Delivery Rev.* **2012**, *64*, 200−216.
(10) He, L.; Huang, Y.; Zhu, H.; Pang, G.; Zheng, W.; Wong, Y. S.; Chen, T. Cancer-Targeted Monodisperse Mesoporous Silica Nanoparticles as Carrier of Ruthenium Polypyridyl Complexes to Enhance Theranostic Effects. *Adv. Funct. Mater.* **2014**, *24*, 2754−2763.
(11) Allen, T. M.; Cullis, P. R. Liposomal Drug Delivery Systems: from Concept to Clinical Applications. *Adv. Drug Delivery Rev.* **2013**, *65*, 36−48.
(12) Weir, A.; Westerhoff, P.; Fabricius, L.; Hristovski, K.; von Goetz, N. Titanium Dioxide Nanoparticles in Food and Personal Care Products. *Environ. Sci. Technol.* **2012**, *46*, 2242−2250.
(13) Fonseca, N. A.; Gregorio, A. C.; Valerio-Fernandes, A.; Simoes, S.; Moreira, J. N. Bridging Cancer Biology and the Patients' Needs with Nanotechnology-Based Approaches. *Cancer Treat. Rev.* **2014**, *40*, 626−635.
(14) Vivek, R.; Thangam, R.; NipunBabu, V.; Rejeeth, C.; Sivasubramanian, S.; Gunasekaran, P.; Muthuchelian, K.; Kannan, S. Multifunctional HER2-Antibody Conjugated Polymeric Nanocarrier-Based Drug Delivery System for Multi-Drug-Resistant Breast Cancer Therapy. *ACS Appl. Mater. Interfaces* **2014**, *6*, 6469−6480.
(15) He, L. Z.; Huang, Y. Y.; Zhu, H. L.; Pang, G. H.; Zheng, W. J.; Wong, Y. S.; Chen, T. F. Cancer-Targeted Monodisperse Mesoporous Silica Nanoparticles as Carrier of Ruthenium Polypyridyl Complexes to Enhance Theranostic Effects. *Adv. Funct. Mater.* **2014**, *24*, 2754−2763.
(16) Chang, H. X.; Wu, H. K. Graphene-Based Nanomaterials: Synthesis, Properties, and Optical and Optoelectronic Applications. *Adv. Funct. Mater.* **2013**, *23*, 984−997.
(17) Beqa, L.; Fan, Z.; Singh, A. K.; Senapati, D.; Ray, P. C. Gold Nano-Popcorn Attached SWCNT Hybrid Nanomaterial for Targeted Diagnosis and Photothermal Therapy of Human Breast Cancer Cells. *ACS Appl. Mater. Interfaces* **2011**, *3*, 3316−3324.
(18) Apartsin, E. K.; Buyanova, M. Y.; Novopashina, D. S.; Ryabchikova, E. I.; Filatov, A. V.; Zenkova, M. A.; Venyaminova, A. G. Novel Multifunctional Hybrids of Single-Walled Carbon Nanotubes with Nucleic Acids: Synthesis and Interactions with Living Cells. *ACS Appl. Mater. Interfaces* **2014**, *6*, 1454−1461.
(19) Zhang, Y.; Bai, Y.; Yan, B. Functionalized Carbon Nanotubes for Potential Medicinal Applications. *Drug Discovery Today* **2010**, *15*, 428−435.
(20) Mulvey, J. J.; Villa, C. H.; McDevitt, M. R.; Escorcia, F. E.; Casey, E.; Scheinberg, D. A. Self-Assembly of Carbon Nanotubes and Antibodies on Tumours for Targeted Amplified Delivery. *Nat. Nanotechnol.* **2013**, *8*, 763−771.
(21) Huang, X. H.; Johnson, R. P.; Song, S. I.; Kim, I. Noncovalent Functionalization of Carbon Nanotubes by Fluorescent Polypeptides: Supramolecular Conjugates with pH-Dependent Absorbance and Fluorescence. *J. Nanosci. Nanotechnol.* **2013**, *13*, 7406−7412.
(22) Liu, Z.; Fan, A. C.; Rakhra, K.; Sherlock, S.; Goodwin, A.; Chen, X.; Yang, Q.; Felsher, D. W.; Dai, H. Supramolecular Stacking of Doxorubicin on Carbon Nanotubes for *In Vivo* Cancer Therapy. *Angew. Chem., Int. Ed.* **2009**, *48*, 7668−7672.
(23) Kang, B.; Li, J.; Chang, S. Q.; Dai, M. Z.; Ren, C.; Dai, Y. D.; Chen, D. Subcellular Tracking of Drug Release from Carbon Nanotube Vehicles in Living Cells. *Small* **2012**, *8*, 777−782.
(24) Yan, W.; Shen, X. C.; Zhang, Z. L.; Chen, C.; Pang, D. W. Electrochemical Behavior of Daunorubicin at DNA-MWCNT Bioconjugates Modified Glassy Carbon Electrodes. *Anal. Lett.* **2005**, *38*, 2579−2595.
(25) Zhang, H. J. Fabrication of a Single-Walled Carbon Nanotube-Modified Glassy Carbon Electrode and Its Application in the Electrochemical Determination of Epirubicin. *J. Nanopart. Res.* **2004**, *6*, 665−669.
(26) Vecchio, D.; Daga, A.; Carra, E.; Marubbi, D.; Baio, G.; Neumaier, C. E.; Vagge, S.; Corvo, R.; Brisigotti, M. P.; Ravetti, J. L.; Zunino, A.; Poggi, A.; Mascelli, S.; Raso, A.; Frosina, G. Predictability, Efficacy and Safety of Radiosensitization of Glioblastoma-Initiating Cells by the ATM Inhibitor KU-60019. *Int. J. Cancer* **2014**, *135*, 479−491.
(27) Shibata, A.; Jeggo, P. A. DNA Double-Strand Break Repair in a Cellular Context. *Clin. Oncol.-UK* **2014**, *26*, 243−249.
(28) Yang, L.; Wang, W. B.; Hu, L.; Yang, X. X.; Zhong, J.; Li, Z.; Yang, H.; Lei, H.; Yu, H. J.; Liao, Z. K.; Zhou, F. X.; Xie, C. H.; Zhou, Y. F. Telomere-Binding Protein TPP1Modulates Telomere Homeostasis and Confers Radioresistance to Human Colorectal Cancer Cells. *PLoS One* **2013**, *8*, e81034.
(29) Oermann, E. K.; Kress, M. A. S.; Todd, J. V.; Collins, B. T.; Hoffman, R.; Chaudhry, H.; Collins, S. P.; Morris, D.; Ewend, M. G. The Impact of Radiosurgery Fractionation and Tumor Radiobiology on the Local Control of Brain Metastases Clinical Article. *J. Neurosurg.* **2013**, *119*, 1131−1138.
(30) Nakazato, T.; Nakanishi, M.; Kita, S.; Okuyama, F.; Shibamoto, Y.; Otsuka, T. Biological Effects of Field Emission-Type X-rays Generated by Nanotechnology. *J. Radiat. Res.* **2007**, *48*, 153−161.
(31) Burke, A. R.; Singh, R. N.; Carroll, D. L.; Wood, J. C. S.; D'Agostino, R. B.; Ajayan, P. M.; Torti, F. M.; Torti, S. V. The Resistance of Breast Cancer Stem Cells to Conventional Hyperthermia and Their Sensitivity to Nanoparticle-Mediated Photothermal Therapy. *Biomaterials* **2012**, *33*, 2961−2970.
(32) Schreiber, E. C.; Chang, S. X. Monte Carlo Simulation of a Compact Microbeam Radiotherapy System Based on Carbon Nanotube Field Emission Technology. *Med. Phys.* **2012**, *39*, 4669−4678.
(33) Singh, R.; Torti, S. V. Carbon Nanotubes in Hyperthermia Therapy. *Adv. Drug Delivery Rev.* **2013**, *65*, 2045−2060.
(34) Wang, S.; Liu, Z.; Sultana, S.; Schreiber, E.; Zhou, O.; Chang, S. A Novel High Resolution Micro-Radiotherapy System for Small Animal Irradiation for Cancer Research. *Biofactors* **2007**, *30*, 265−270.
(35) Romero-Canelon, I.; Sadler, P. J. Next-Generation Metal Anticancer Complexes: Multitargeting via Redox Modulation. *Inorg. Chem.* **2013**, *52*, 12276−12291.
(36) Micallef, L. S.; Loughrey, B. T.; Healy, P. C.; Parsons, P. G.; Williams, M. L. Synthesis, Spectroscopic Characterization, and Cytotoxic Evaluation of Pentasubstituted Ruthenocenyl Esters. *Organometallics* **2010**, *29*, 6237−6244.
(37) Chen, T.; Liu, Y.; Zheng, W. J.; Liu, J.; Wong, Y. S. Ruthenium Polypyridyl Complexes that Induce Mitochondria-Mediated Apoptosis in Cancer Cells. *Inorg. Chem.* **2010**, *49*, 6366−6368.
(38) Yu, B.; Zhang, Y.; Zheng, W.; Fan, C.; Chen, T. Positive Surface Charge Enhances Selective Cellular Uptake and Anticancer Efficacy of Selenium Nanoparticles. *Inorg. Chem.* **2012**, *51*, 8956−8963.
(39) Chen, T.; Wong, Y. S. Selenocystine Induces Apoptosis of A375 Human Melanoma Cells by Activating ROS-Mediated Mitochondrial Pathway and p53 Phosphorylation. *Cell. Mol. Life Sci.* **2008**, *65*, 2763−2775.
(40) Kang, B.; Yu, D.; Dai, Y.; Chang, S.; Chen, D.; Ding, Y. Cancer-Cell Targeting and Photoacoustic Therapy Using Carbon Nanotubes as "Bomb" Agents. *Small* **2009**, *5*, 1292−1301.
(41) Wilhelmsson, L. M.; Westerlund, F.; Lincoln, P.; Norden, B. DNA-Binding of Semirigid Binuclear Ruthenium Complex delta,delta-$[\mu$-(11,11′-bidppz)$(phen)_4Ru_2]^{4+}$: Extremely Slow Intercalation Kinetics. *J. Am. Chem. Soc.* **2002**, *124*, 12092−12093.
(42) Huang, Y.; He, L.; Liu, W.; Fan, C.; Zheng, W.; Wong, Y. S.; Chen, T. Selective Cellular Uptake and Induction of Apoptosis of

DOI: 10.1021/acsami.5b03739
ACS Appl. Mater. Interfaces 2015, 7, 14933−14945

Cancer-Targeted Selenium Nanoparticles. *Biomaterials* **2013**, *34*, 7106−7116.
(43) Chen, T.; Wong, Y. S. Selenocystine Induces Caspase-Independent Apoptosis in MCF-7 Human Breast Carcinoma Cells with Involvement of p53 Phosphorylation and Reactive Oxygen Species Generation. *Int. J. Biochem. Cell Biol.* **2009**, *41*, 666−676.
(44) Pulskamp, K.; Diabate, S.; Krug, H. F. Carbon Nanotubes Show No Sign of Acute Toxicity but Induce Intracellular Reactive Oxygen Species in Dependence on Contaminants. *Toxicol. Lett.* **2007**, *168*, 58−74.
(45) Kagan, V. E.; Tyurina, Y. Y.; Tyurin, V. A.; Konduru, N. V.; Potapovich, A. I.; Osipov, A. N.; Kisin, E. R.; Schwegler-Berry, D.; Mercer, R.; Castranova, V.; Shvedova, A. A. Direct and Indirect Effects of Single Walled Carbon Nanotubes on RAW 264.7 Macrophages: Role of Iron. *Toxicol. Lett.* **2006**, *165*, 88−100.
(46) Lozano, R.; Naghavi, M.; Foreman, K.; Lim, S.; Shibuya, K.; Aboyans, V.; Abraham, J.; Adair, T.; Aggarwal, R.; Ahn, S. Y.; Alvarado, M.; Anderson, H. R.; Anderson, L. M.; Andrews, K. G.; Atkinson, C.; Baddour, L. M.; Barker-Collo, S.; Bartels, D. H.; Bell, M. L.; Benjamin, E. J.; Bennett, D.; Bhalla, K.; Bikbov, B.; Bin Abdulhak, A.; Birbeck, G.; Blyth, F.; Bolliger, I.; Boufous, S. A.; Bucello, C.; Burch, M.; Burney, P.; Carapetis, J.; Chen, H. L.; Chou, D.; Chugh, S. S.; Coffeng, L. E.; Colan, S. D.; Colquhoun, S.; Colson, K. E.; Condon, J.; Connor, M. D.; Cooper, L. T.; Corriere, M.; Cortinovis, M.; de Vaccaro, K. C.; Couser, W.; Cowie, B. C.; Criqui, M. H.; Cross, M.; Dabhadkar, K. C.; Dahodwala, N.; De Leo, D.; Degenhardt, L.; Delossantos, A.; Denenberg, J.; Des Jarlais, D. C.; Dharmaratne, S. D.; Dorsey, E. R.; Driscoll, T.; Duber, H.; Ebel, B.; Erwin, P. J.; Espindola, P.; Ezzati, M.; Feigin, V.; Flaxman, A. D.; Forouzanfar, M. H.; Fowkes, F. G. R.; Franklin, R.; Fransen, M.; Freeman, M. K.; Gabriel, S. E.; Gakidou, E.; Gaspari, F.; Gillum, R. F.; Gonzalez-Medina, D.; Halasa, Y. A.; Haring, D.; Harrison, J. E.; Havmoeller, R.; Hay, R. J.; Hoen, B.; Hotez, P. J.; Hoy, D.; Jacobsen, K. H.; James, S. L.; Jasrasaria, R.; Jayaraman, S.; Johns, N.; Karthikeyan, G.; Kassebaum, N.; Keren, A.; Khoo, J. P.; Knowlton, L. M.; Kobusingye, O.; Koranteng, A.; Krishnamurthi, R.; Lipnick, M.; Lipshultz, S. E.; Ohno, S. L.; Mabweijano, J.; MacIntyre, M. F.; Mallinger, L.; March, L.; Marks, G. B.; Marks, R.; Matsumori, A.; Matzopoulos, R.; Mayosi, B. M.; McAnulty, J. H.; McDermott, M. M.; McGrath, J.; Mensah, G. A.; Merriman, T. R.; Michaud, C.; Miller, M.; Miller, T. R.; Mock, C.; Mocumbi, A. O.; Mokdad, A. A.; Moran, A.; Mulholland, K.; Nair, M. N.; Naldi, L.; Narayan, K. M. V.; Nasseri, K.; Norman, P.; O'Donnell, M.; Omer, S. B.; Ortblad, K.; Osborne, R.; Ozgediz, D.; Pahari, B.; Pandian, J. D.; Rivero, A. P.; Padilla, R. P.; Perez-Ruiz, F.; Perico, N.; Phillips, D.; Pierce, K.; Pope, C. A.; Porrini, E.; Pourmalek, F.; Raju, M.; Ranganathan, D.; Rehm, J. T.; Rein, D. B.; Remuzzi, G.; Rivara, F. P.; Roberts, T.; De Leon, F. R.; Rosenfeld, L. C.; Rushton, L.; Sacco, R. L.; Salomon, J. A.; Sampson, U.; Sanman, E.; Schwebel, D. C.; Segui-Gomez, M.; Shepard, D. S.; Singh, D.; Singleton, J.; Sliwa, K.; Smith, E.; Steer, A.; Taylor, J. A.; Thomas, B.; Tleyjeh, I. M.; Towbin, J. A.; Truelsen, T.; Undurraga, E. A.; Venketasubramanian, N.; Vijayakumar, L.; Vos, T.; Wagner, G. R.; Wang, M. R.; Wang, W. Z.; Watt, K.; Weinstock, M. A.; Weintraub, R.; Wilkinson, J. D.; Woolf, A. D.; Wulf, S.; Yeh, P. H.; Yip, P.; Zabetian, A.; Zheng, Z. J.; Lopez, A. D.; Murray, C. J. L. Global and Regional Mortality from 235 Causes of Death for 20 Age Groups in 1990 and 2010: a Systematic Analysis for the Global Burden of Disease Study 2010. *Lancet* **2012**, *380*, 2095−2128.
(47) Wray, C. J.; Harvin, J. A.; Silberfein, E. J.; Ko, T. C.; Kao, L. S. Pilot Prognostic Model of Extremely Poor Survival Among High-Risk Hepatocellular Carcinoma Patients. *Cancer-Am. Cancer Soc.* **2012**, *118*, 6118−6125.
(48) Moskowitz, A. J.; Yahalom, J.; Kewalramani, T.; Maragulia, J. C.; Vanak, J. M.; Zelenetz, A. D.; Moskowitz, C. H. Pretransplantation Functional Imaging Predicts Outcome Following Autologous Stem Cell Transplantation for Relapsed and Refractory Hodgkin Lymphoma. *Blood* **2010**, *116*, 4934−4937.
(49) Katakami, N.; Tada, H.; Mitsudomi, T.; Kudoh, S.; Senba, H.; Matsui, K.; Saka, H.; Kurata, T.; Nishimura, Y.; Fukuoka, M. A Phase 3 Study of Induction Treatment with Concurrent Chemoradiotherapy Versus Chemotherapy Before Surgery in Patients with Pathologically Confirmed N2 Stage IIIA Nonsmall Cell Lung Cancer (WJTOG9903). *Cancer-Am. Cancer Soc.* **2012**, *118*, 6126−6135.
(50) Qin, H.; Luo, J.; Zhu, Y. P.; Xie, H. L.; Yang, W. Q.; Lei, W. B. Combination of Taxanes, Cisplatin and Fluorouracil as Induction Chemotherapy for Locally Advanced Head and Neck Cancer: A Meta-Analysis. *PLoS One* **2012**, *7*, e51526.
(51) Prestwich, R. J. D.; Kancherla, K.; Oksuz, D. C.; Williamson, D.; Dyker, K. E.; Coyle, C.; Sen, M. A Single Centre Experience with Sequential and Concomitant Chemoradiotherapy in Locally Advanced Stage IV Tonsillar Cancer. *Radiat. Oncol.* **2010**, *5*, 1−10.
(52) Dwyer, D. J.; Camacho, D. M.; Kohanski, M. A.; Callura, J. M.; Collins, J. J. Antibiotic-Induced Bacterial Cell Death Exhibits Physiological and Biochemical Hallmarks of Apoptosis. *Mol. Cell* **2012**, *46*, 561−572.
(53) Sen, F.; Boghossian, A. A.; Sen, S.; Ulissi, Z. W.; Zhang, J. Q.; Strano, M. S. Observation of Oscillatory Surface Reactions of Riboflavin, Trolox, and Singlet Oxygen Using Single Carbon Nanotube Fluorescence Spectroscopy. *ACS Nano* **2012**, *6*, 10632−10645.
(54) Wang, J. Y.; Sun, P. P.; Bao, Y. M.; Dou, B. R.; Song, D. D.; Li, Y. C. Vitamin E Renders Protection to PC12 Cells against Oxidative Damage and Apoptosis Induced by Single-Walled Carbon Nanotubes. *Toxicol. in Vitro* **2012**, *26*, 32−41.

DOI: 10.1021/acsami.5b03739
ACS Appl. Mater. Interfaces 2015, 7, 14933−14945